DOUBLE STATOR WINDING INDUCTION GENERATOR FOR RENEWABLE ENERGY CONVERSION SYSTEMS

Adrian D. MARTIN, Dănuț L. VITAN, Lucian N. TUTELEA, Nicolae MUNTEAN
Electrical Engineering Department, Politehnica University of Timișoara
Timișoara, Romania
vitan.danut@gmail.com lucian.tutelea@upt.ro

Abstract: *The paper presents a double stator winding induction generator (DSWIG) used in renewable energy systems. The generator has a squirrel-cage rotor and a two separate stator windings. The main winding is connected to a DC bus through an inverter. The auxiliary winding is connected to a capacitor bank, in order to ensure a part of the necessary reactive power, in parallel with an unpretentious (resistive) load. At low speed the inverter produces the required reactive power necessary for magnetization. At high speed, the reactive power of the capacitor bank is considerable, reducing the apparent power of the inverter. A designing method for the capacitor bank is presented, considering the self excitation phenomenon.*

Key words: *Induction Generator, Renewable Energies, Excitation Control.*

1. Introduction

The cage-type induction generators represent an advantageous solution due to their main advantages: good dynamic performance, brushless, no additional power DC sources, low maintenance demands and good overload protection ability [1]-[3].

When the induction generator is connected directly to the grid, it works at approximately constant speed. These kinds of energy systems require a turbine with adjustable parameters, which is hard to realize and expensive at low power [4]. Other drawbacks are related to the difficulty to adjust the reactive power and the poor performance of the output voltage [5]. A fully controllable generator for variable speed turbine can be made using an inverter (Fig. 1). In this configuration the inverter needs to be designed at rated power.

An alternative could be a wound rotor induction generator, connected through a "back-to-back" converter to the grid, in parallel with the stator windings, in so called DFIG system, as presented in Fig. 2 [6]-[8]. The apparent power of the inverter in this case is 25% smaller compared with the structure on Fig. 1, but the brushes are the main disadvantage of this scheme.

The solution presented in this paper is a split wound induction machine, where the stator has two three-phase windings, with the same poles pair number (DSWIG).

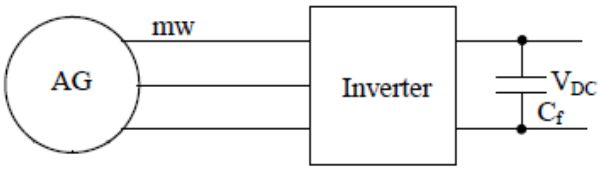

Fig. 1. The proposed solution for traditional induction generator

DSWIG was introduced by T.F. Barton since 1927 and developed by Ph. L. Alger [9]. Fig. 3 shows two different typologies using a DSWIG.

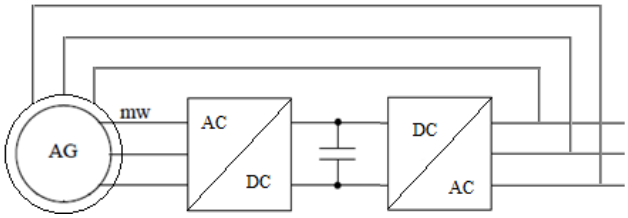

Fig. 2. DFIG system

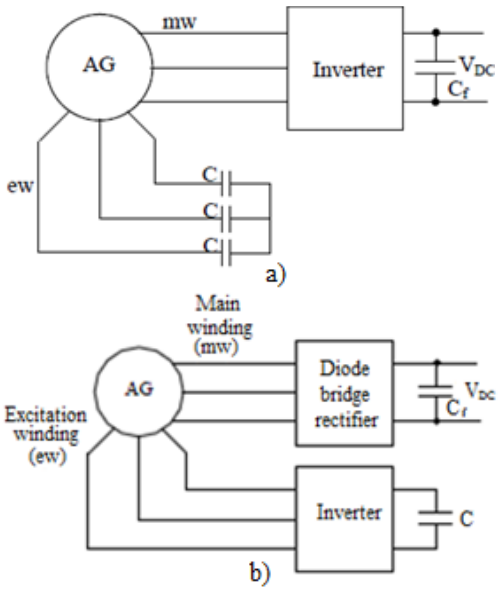

Fig. 3. DSWIG power generation schemes: a) two stator three-phase windings and reactive power compensation; b) solution for variable reactive power

In the first case (Fig. 3a) the excitation phase is directly connected to a fixed capacitor bank, and the apparent power is reduced up to 40%. In the second case (Fig. 3b) a voltage source inverter is used to provide variable reactive power.

The self-excited phenomenon must be taken into consideration when choosing the capacitors. In Fig. 3b the main winding is directly connected to a rectifier bridge, and carries all the active power. The auxiliary winding is design for a higher voltage in order to reduce the inverter current. In Fig. 3a the excitation winding ensures only the reactive power, and the main winding can give both active and reactive power. In Fig. 3b the main winding gives only active power [10]-[11].

In a DSWIG the windings are mutually coupled, with different inductances due to their position within the slots. In the presented case the stator windings are placed in the same slots.

The DSWIG windings have a larger weight and volume than the classical induction generator, but in variable speed and load, encountered in both wind and hydro turbines of low power, the performance and total cost of DSWIG and static converter are improved.

An active rectifier (on the main winding) and a diode rectifier (on the auxiliary winding) are used for a better utilization of copper (Fig. 4). Both are design for half of the rated power. The auxiliary winding is connected to the DC bus through a three phase inductances and a diode rectifier. At low speeds only the main winding supplies energy to the DC bus. At high speed both windings deliver into the DC bus. In this case, the inverter can control the active and reactive power distribution in the DSWIG windings.

In the proposed solution a part of the power is delivered directly to some AC unpretentious loads that are connected to the auxiliary winding (Fig. 5).

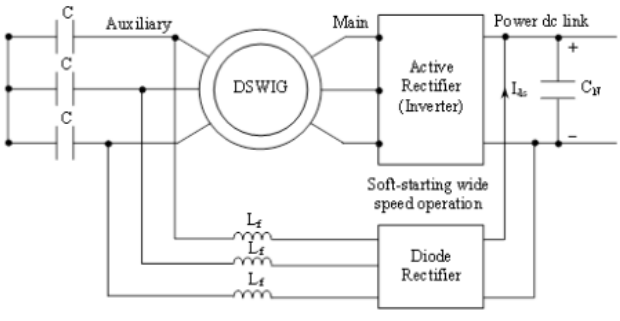

Fig. 4. DSWIG with active rectifier on main winding and diode rectifier on auxiliary winding

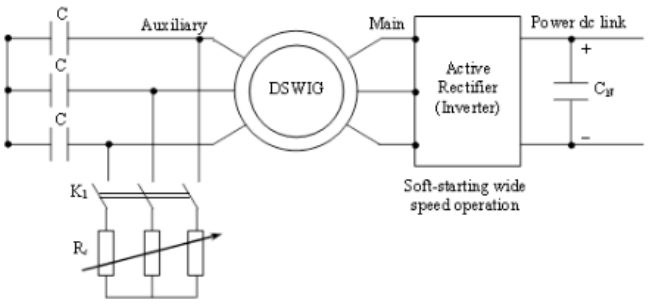

Fig. 5. The proposed solution configuration

For example, in a wind turbine the unpretentious loads will be connected only when the available energy is larger than 50% of the rated power which means that the turbine speed will be larger than 80% of the rated speed.

In the next sections an analytical description of DSWIG is presented. Then the capacitor bank is designed. Finally, digital simulation and experimental results, performed on a laboratory setup, validate the theoretical considerations.

2. DSWIG - equivalent scheme and equations

In the dynamic model of DSWIG the excitation and rotor winding parameters are reduced to the main winding. Equivalent electrical diagram of DSWIG, including unpretentious loads, is shown in Fig 6.

The steady state equation (1) is presented in matrix form for sinusoidal currents, were:

-V_2 is the auxiliary voltage;

-V'_2 is the phase auxiliary voltage related to the main winding;

- I'_2 is the phase auxiliary current related to the main winding;

- k is the related factor;

- k_{w1} and k_{w2} are the winding factor;

- $L_1\sigma$ and R_1 are the leakage inductance and resistance of the main winding;

- $L'_2\sigma$ and R_2 are the auxiliary leakage inductance and resistance related to the main winding;

- $L_{12}\sigma$ is the leakage inductance of the main and auxiliary windings;

- L_m is the magnetization inductance;

- $L'_r\sigma$ and R'_r are the rotor leakage inductance and resistance related to the main winding;

- C' is the capacitor bank related to the main winding;

- R'_s is the auxiliary load;

- P_{mec} corresponds to the mechanical losses.

$$\begin{bmatrix}\underline{V_1}\\ \underline{V_2'}\\ 0\end{bmatrix}=\begin{bmatrix}R_1+j\omega_1(L_{1\sigma}+L_{12\sigma}+L_m) & j\omega_1(L_{12\sigma}+L_m) & j\omega_1 L_m\\ j\omega_1(L_{12\sigma}+L_m) & R_2+j\omega_1(L_2+L_{12\sigma}+L_m) & j\omega_1 L_m\\ j\omega_1 L_m & j\omega_1 L_m & \frac{R_r}{s}+j\omega_1(L_{r\sigma}+L_m)\end{bmatrix}\begin{bmatrix}\underline{I_1}\\ \underline{I_2'}\\ \underline{I_r'}\end{bmatrix}, \quad (1)$$

$$V_2'=k\cdot V_2;\ \ I_2'=\frac{I_2}{k};\ \ k=\frac{V_{1e}}{V_{2e}}=\frac{N_1\cdot k_{w1}}{N_2\cdot k_{w2}}, \quad (2)$$

$$L_{2\sigma}'=k^2\cdot L_{1\sigma};\ R_2'=k^2\cdot R_2, \quad (3)$$

$$C'=\frac{1}{k^2}\cdot C, \quad (4)$$

$$\underline{V}=\underline{Z}\cdot\underline{I};\ \underline{I_a}=\underline{Z}^{-1}\cdot\underline{V}, \quad (5)$$

$$\underline{V_{C0}'}=-\frac{1}{j\omega_1 C'}\cdot\underline{I_{2a}'}, \quad (6)$$

$$R_s'=k^2\cdot R_s, \quad (7)$$

$$\underline{V_{C0}'}=-R_s'\cdot\underline{I_{2b}'}, \quad (8)$$

$$\underline{I_2'}=-\underline{I_{2a}'}-\underline{I_{2b}'}, \quad (9)$$

The DSWIG parameters are presented in the next table [12]. They were determined with the unsaturated machine core.

Table 1. The DSWIG parameters

Variable	Value
k	0.99
R_1	4.2 [Ω]
R_2	2.5 [Ω]
R_r	2.2 [Ω]
R_m	1418 [Ω]
$L_1\sigma$	0.95 [mH]
$L_2\sigma$	12.54 [mH]
$L_{12}\sigma$	23.41 [mH]
$L_r\sigma$	9.03 [mH]
Lm	345.44 [mH]
P_{mec}	58 [W]

The capacitor bank must be designed in order to offer enough reactive power, but at the same time not too much as to create self-excited phenomenon.

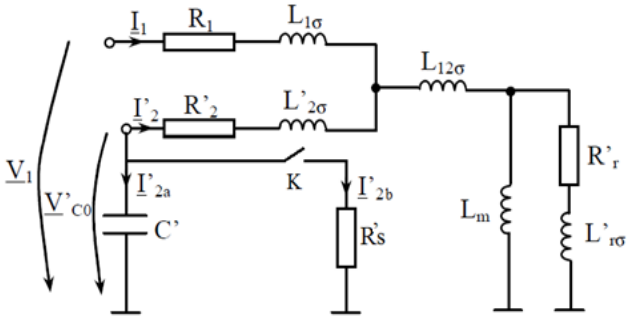

Fig 6. DSWIG with resistance and capacitor on the excitation phase

3. The reactive power compensation

A capacitor bank is used to compensate the reactive power. Equation (10) shows the capacity computation considering that all reactive power is produced by the capacitor bank.

$$Q=3\cdot U_e^2\cdot\omega\cdot C \Rightarrow C=\frac{Q}{3\cdot U_e^2\cdot\omega}, \quad (10)$$

At $\omega_1=200$ [rad/s], ($n=477{,}7\left[\frac{rot}{min}\right], f=31.84\,[Hz]$), the induction machine required a reactive power Q=720 [VAR].

In this case the capacity is $C=94.76\,[\mu F]$;

On the another hand, the self-excited phenomenon should be avoid which means that the next condition is accomplished:

$$X_C\geq X_L \Rightarrow \frac{1}{\omega_1\cdot C}\geq\omega_1\cdot L, \quad (11)$$

$$C\leq\frac{1}{\omega_1^2\cdot L}, \quad (12)$$

According to the Table 1 values, the capacity is computed to avoid the self-excited phenomenon at ω_1=200[rad/s].

$$L_L=L_{2\sigma}+L_{12\sigma}+L_m=0.38\,[H], \quad (13)$$

For $X_C=X_L$ we obtain

$$C=\frac{1}{\omega_1^2\cdot L} \Rightarrow C=65.5\,[\mu F];$$

A smaller value (C = 60 [μF]), was chosen in order to secure the system against self-excitation phenomenon.

The energy stored in capacitors must be lower than the magnetization energy. This fact is shown below:

$$\omega_1=200\left[\frac{rad}{s}\right] \Rightarrow f=31{,}84\,[Hz] \Rightarrow 60\cdot10^{-6}<65{,}54\cdot10^{-6}; \quad (14)$$

$$\omega_1=210\left[\frac{rad}{s}\right] \Rightarrow f=33{,}43\,[Hz] \Rightarrow 60*10^{-6}>59{,}45\cdot10^{-6}; \quad (15)$$

From previous calculations is observed that up to a speed of 200 [rad/s] the capacitor can't provide enough reactive energy to excite the machine. The self-excited danger appears only over this rotation speed.

The self-excited phenomenon was simulated in Matlab / Simulink with DSWIG as generator, with a large resistance connected to the main winding terminals: R_{load}=1500 [Ω], and the capacitor battery connected to the auxiliary winding terminals (Fig. 7). There have been introduced various values of capacitors to view the behavior of the machine at 200 [rad/s].

The saturated model of the machine (16) was tuned from magnetization inductance observed from FEM (finite element method) simulation.

In this way it could get the high sinusoidal voltage necessary to determine the inductances.

$$L_m = \left(\frac{k_{lsat1}\cdot I_{ev}^2+1}{k_{lsat3}\cdot I_{ev}^3+k_{lsat2}\cdot I_{ev}^2}\right)\cdot L_{m0}, \quad (16)$$

$$\sum L = L_m + L_{2\sigma} + L_{12\sigma}, \quad (17)$$

where I_{ev} represent the peak auxiliary current.

Fig. 8 shows the self-excited phenomenon obtained from simulation, at ω = 212.8 [rad/s], C = 60 [μF].

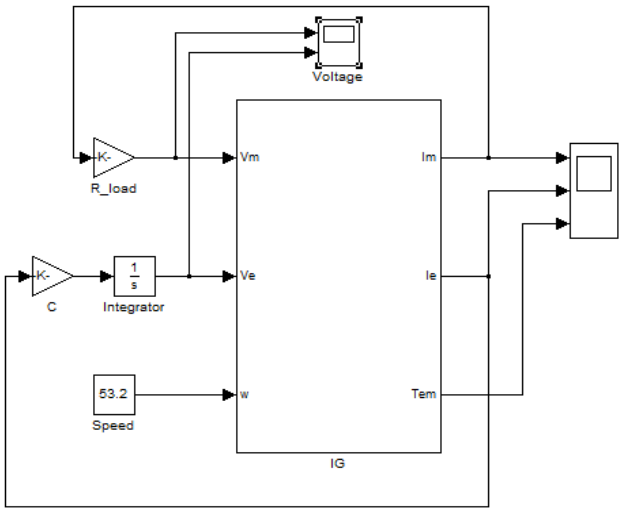

Fig. 7. The Simulink block diagram to simulate self-excited phenomenon

The self-excitation phenomenon is strongly dependent on the magnetization inductance nonlinearity and a test validation was necessary. The experiments were carried out with a double capacity value in order to reduce the terminal voltage, for safety reason. The self-excited phenomenon occurs at lower speed. The following charts show the self-excited phenomenon obtained from measurements, for ω = 155.32[rad/s], C=120 [μF] – Fig. 9.

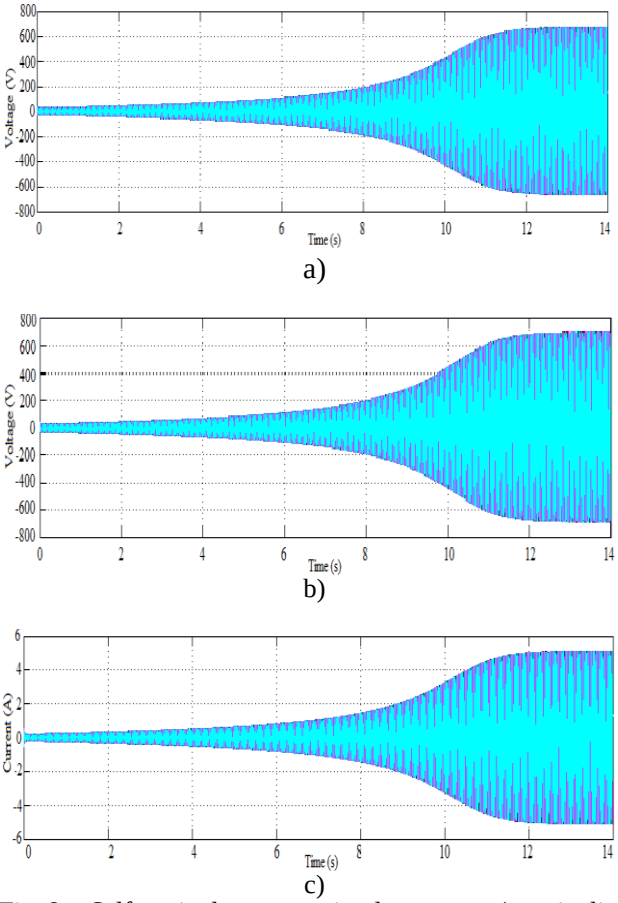

Fig. 8. Self-excited process simulate case: a) main line voltage, b) auxiliary line voltage, c) auxiliary current

The auxiliary voltage winding increases with the speed, as it is shown in Fig. 10 where significant difference between test and simulation voltage (Sim 1) could be observed. This error is produced by the difference from the magnetization inductance curve obtained from FEM, and the real one. Fortunately, a new magnetization inductance curve could be computed from the self-excited test (Fig.11).

In the following chart, the blue curve represents the actual voltage obtained in the laboratory. With this one was calculated the inductance versus to the current amplitude (18). In Fig. 11 it can be noted comparison between inductance obtained from FEM (Sim1 curve) and another inductance obtained from calculations (the blue one).

$$L_m + L_{2\sigma} + L_{12\sigma} = \frac{U_{ef}}{\omega_{el}*I_e}, \quad (18)$$

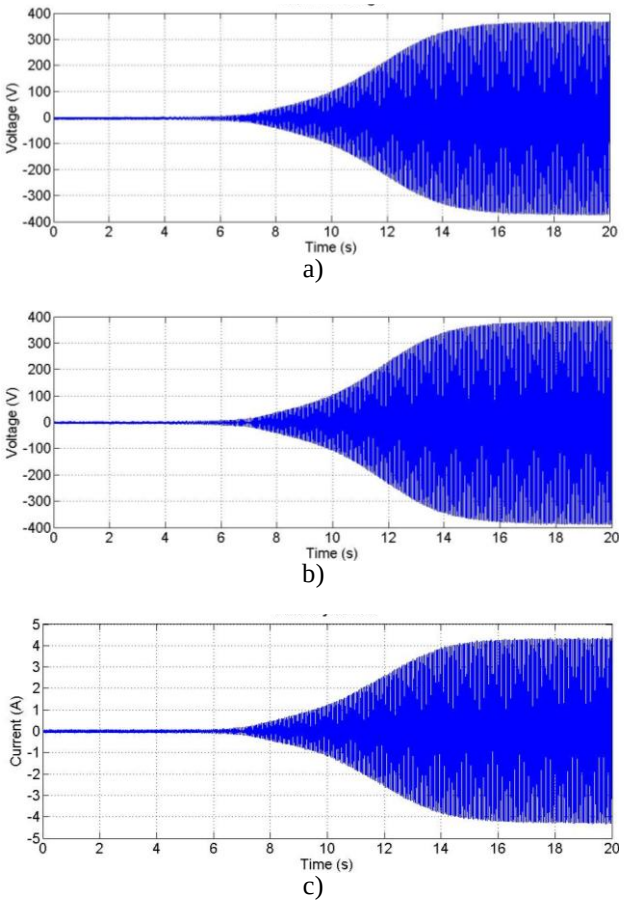

Fig. 9. Self-excited process real case: a) main line voltage, b) auxiliary line voltage, c) auxiliary current.

With the magnetization inductance from the experiments the coefficients of the new magnetization inductance were recalculated. They are presented in Table 2.

With these new coefficients, the simulation was repeated for a capacity of 60[uF] and it was observed that the self-excited phenomenon occurs at a speed greater than 200[rad/s].

Table 2. The magnetization inductance coefficients (16)

The coefficients	Sim1 (FEM)	Sim 2
k_{lsat1}	0.03	0.0195
k_{lsat2}	0.0137	0.0197
k_{lsat3}	0.0036	0.0018

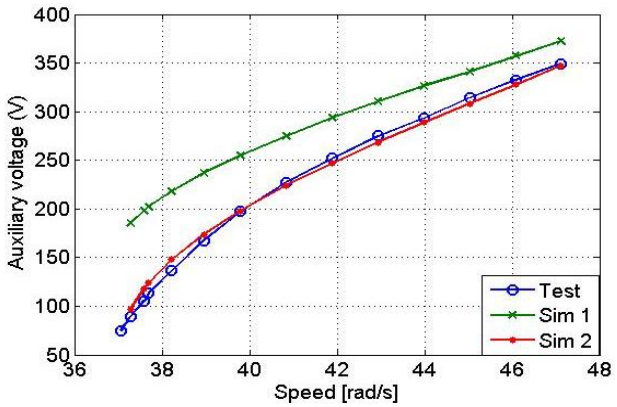

Fig. 10. Auxiliary winding voltage: Sim 1- obtained from FEM, Sim 2- obtained by changing the coefficients

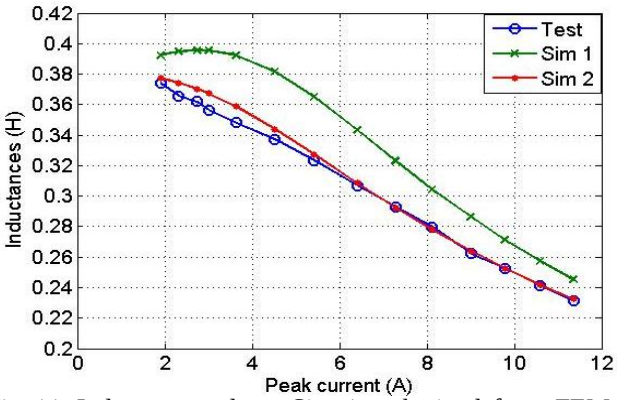

Fig. 11. Inductance values: Sim 1 - obtained from FEM, Sim 2 - obtained from self-excited test.

4. Load operation of DSWIG

The capacitor battery supplies the DSWIG with almost the entire reactive power at the maximum speed and no load operation, this way the total apparent power of the inverter is reduced. At low speed the capacitor battery offer less reactive power, but the inverter still magnetize the generator.

In the next figures is represented the influence of the capacitor value on reactive power consumption.

In this experiment, the wind turbine was emulated by a 11 [KW] induction motor driven by a bidirectional inverter. The inverter has limitation in current, speed, and torque, with the possibilities to prescribe the needed torque. The rated torque of the drive motor is denoted with *Mn* and it is equal with 140[Nm]. This fact is used to load the DSWIG at different torques and speeds. The active power from the inverter doesn't depend on the capacitor bank presence (Fig.12), while the reactive power is decreasing when capacitor bank is connected (Fig.13).

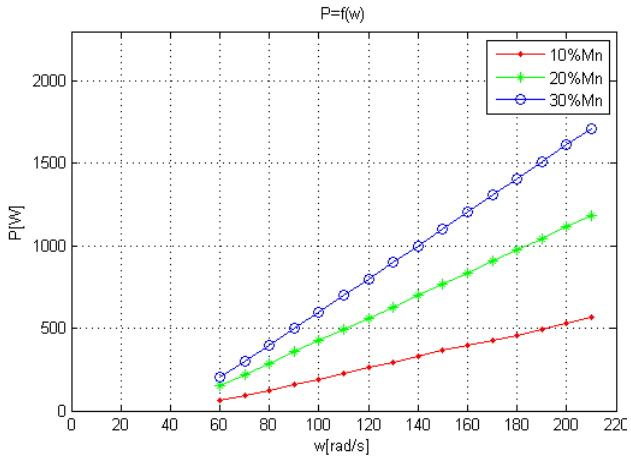

a)

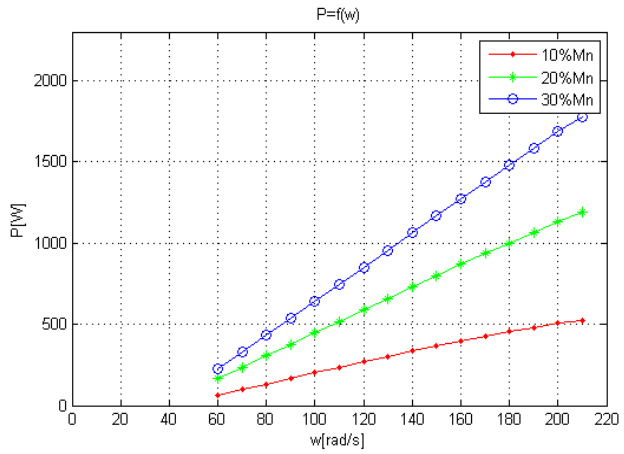

b)

Fig. 12. Active power generated by DSWIG: a) without capacitor battery, b) with capacitor battery

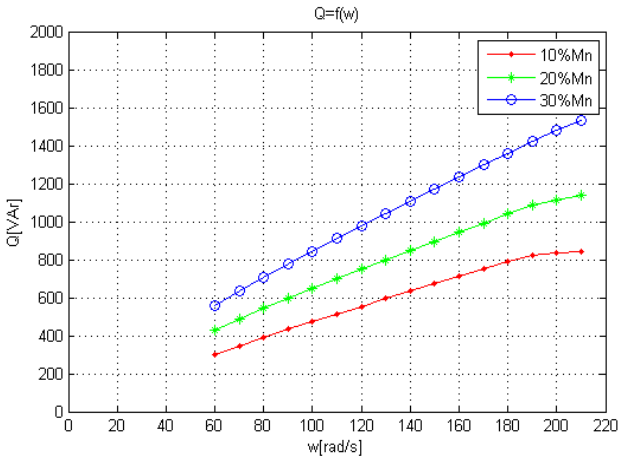

a)

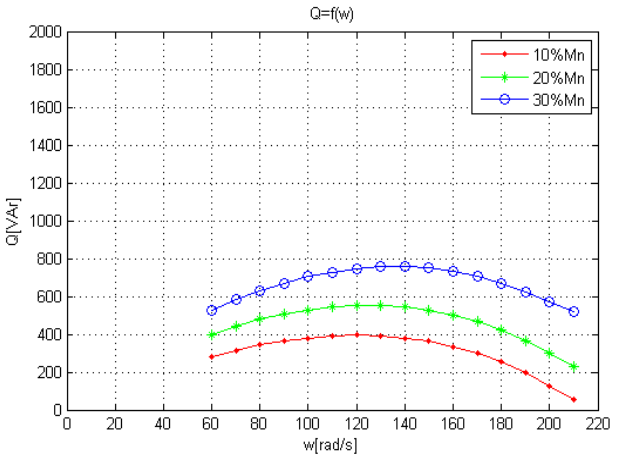

b)

Fig. 13. Reactive power absorbed by DSWIG through inverter: a) without capacitor battery, b) with capacitor battery

The DSWIG capability to generate different active power on the two windings was proven in laboratory test, at different speeds. The capacitor battery still remains connected to the auxiliary winding, in parallel with unpretentious load. The test results can be seen in the following graphs.

The test results without capacitor battery at speed $\omega = 190\ \left[\frac{rad}{s}\right]$, drive torque M=30%Mn [Nm] and R_{load}=110[Ω] is shown in Fig.14. The powers measured during this experiment are:

- the power on the resistance=844 [W];
- the power delivered to the DC bus=661 [W];
- the reactive power through the inverter= 1421[VAR];

The test results with capacitor battery at $\omega = 190\ \left[\frac{rad}{s}\right]$, drive torque M=30%Mn [Nm] and R_{load}=110[Ω] is shown in Fig.15. The powers measured during this experiment are:

- the power on the resistance=792[W];
- the power on the electronic load=700[W];
- the reactive power through inverter = 811[VAR];

The DC voltage source is used to power the DSWIG as a motor, through the inverter. The drive motor spins the DSWIG as a generator. When the DC voltage is greater than the DC source voltage, the diode D is blocked.

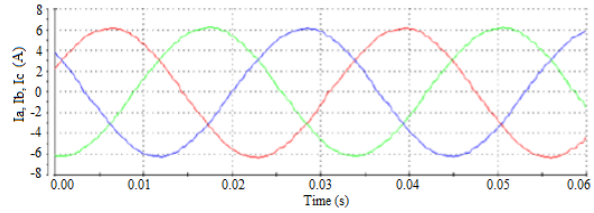

a)

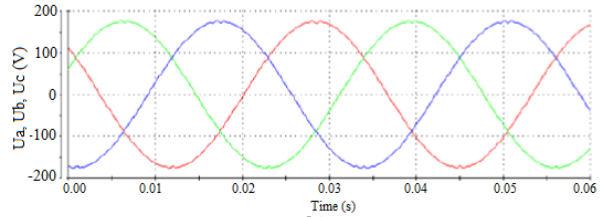

b)

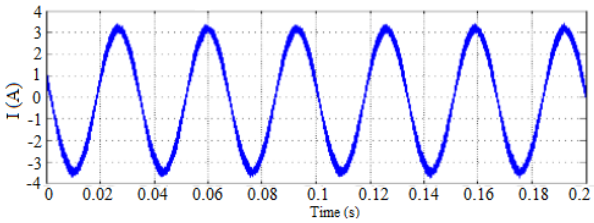

c)

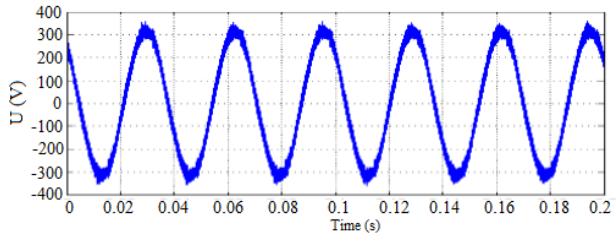

d)

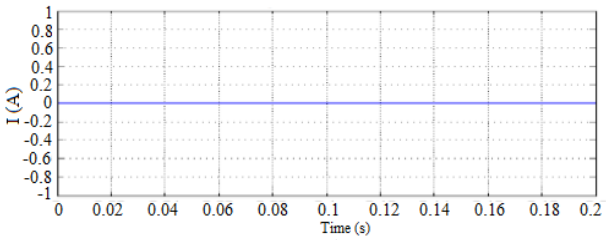

e)

Fig. 14. Experimental results without capacitors: a) the main winding currents, b) the main winding voltage, c) the resistive load current, d) the induced line voltage, e) the capacitor current;

The generated power at the main winding of DSWIG is consumed by electronic load. This electronic load has voltage, current and power limitation, and is operating in constant voltage mode.

The test setup is presented in Fig. 16.

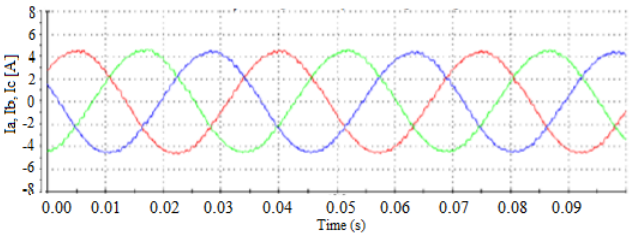

a)

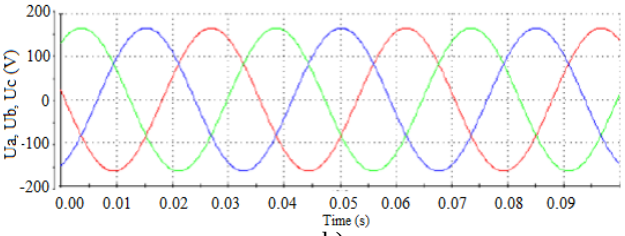

b)

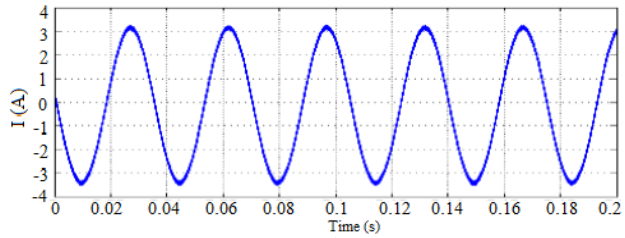

c)

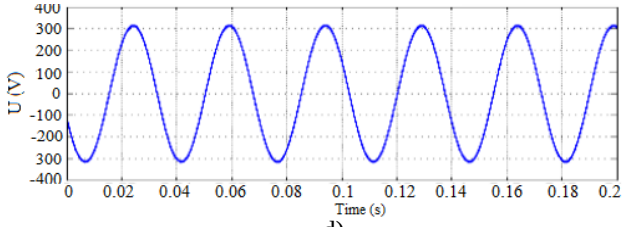

d)

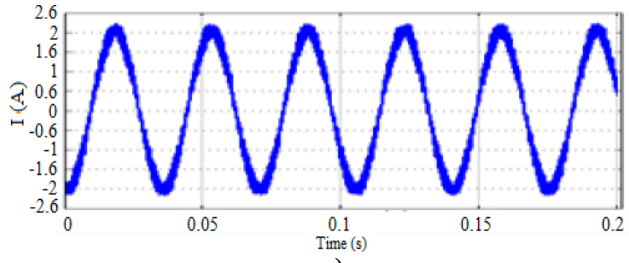

e)

Fig. 15. Experimental results with capacitors: a) the main winding currents, b) the main winding voltage, c) the resistive load current, d) the induced line voltage, e) the capacitor current;

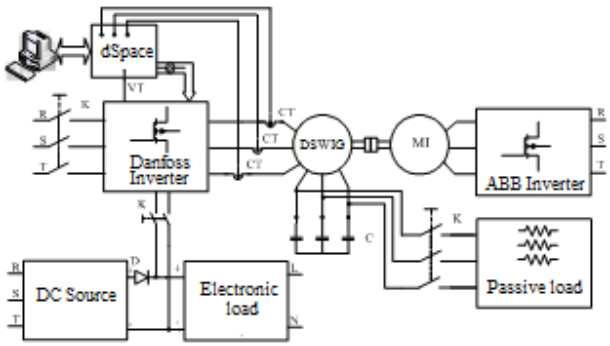

Fig. 16. The block diagram of the experimental setup

5. Conclusion

The DSWIG scheme proposed in this paper uses an inverter with apparent power less than the corresponding generator power.

The expected ratio between the inverter power and the generator power is 50% in DSWIG case.

This is similar to DFIG applications.

The advantage of DSWIG is given by the lack of brushes.

DSWIG can be used in variable speed applications. It is possible to extract a low power even at low speeds, which cannot be obtained in the case when the generator is directly connected to the grid, or when the generator has an inverter on the excitation winding and a diode bridge on the main winding.

The DSWIG studied typology is an advantageous solution when it supplies unpretentious loads.

The inverter on the main winding is used to transfer active power and also reactive power required for generator magnetization at low speeds, when the capacitor could not provide enough reactive power.

A method to determine the saturated inductance of the DSWIG was also developed.

Digital simulations and experimental results, in good correspondence, prove the validity of the theoretical considerations.

Acknowledgment

This paper was supported by the project "Microgrid integrated small power renewable energy hybrid systems" PCCA 36/2012, PN-II-PCCA-2011-3.2-1519, Funding Application for Joint Applied Research Projects

References

1. K. K. Mohapatra et al., "*Independent field-oriented control of two splitphase induction motors from a single six-phase inverter*," IEEE Trans. Ind. Electron., vol. 52, no. 5, Oct. 2005, pp. 1372–1382.
2. E. A. Klingshirn, "*Harmonic filters for six-phase and other multi phase motors on voltage source inverter*," IEEE Trans. Ind. Appl., vol. 1A-21, no. 4, May/Jun. 1985, pp. 588–593.
3. Y. Zhao and T. A. Lipo, "*Space vector PWM control of dual three-phase induction machine using space vector decomposition*," IEEE. Trans. Ind. Appl., vol. 31, no. 5, Sep./Oct. 1995, pp. 1100–1109.
4. O. Ojo, I.E. Davidson, "*PWM-VSI inverter-assisted stand-alone dual stator winding generator*", IEEE Transaction on Industry Applications, vol. 36, no. 6, Nov./Dec. 2000, pp. 1604-1611.
5. Jabri, A.K.A., and Alolah, A.I., "*Limits on the performance of the three-phase self-excited induction generators*", IEEE Transaction on Energy Conversion, vol. 5, no. 2, Jun. 1990, pp. 350–356.
6. L.H. Hansen, L. Hellen, F. Blaabjerg, E. Rithcie, S. Munk-Nielsen, H. Bindner, P. Sørensen and B. Bak-Jensen, "*Conceptual survey of Generators and Power Electronics for Wind Turbines*", Risø-R-1205(EN), Risø National Laboratory, Roskilden, Denmark, December 2001.
7. S. Basak, C. Chakraborty, "*Dual Stator Winding Induction Machine: Problems, Progress, and Future Scope"* , IEEE Trans. on Ind. Electronics, vol.62, no.7, July 2015, pp. 4641-4652.
8. T. Long, S. Shao, P. Malliband, E. Abdi, and R. A. McMahon, "*Crowbarless fault ride-through of the brushless doubly fed induction generator in a wind turbine under symmetrical voltage dips,"* IEEE Trans. Ind. Electron., vol. 60, no. 7, Jul. 2013, pp. 2833–2841.
9. P. L. Alger, E. H. Freiburghouse, and D. D. Chase, "*Double windings for turbine alternators*", AIEE Trans., vol.49, Jan. 1930, pp. 226-244.
10. L. N. Tutelea, S. I. Deaconu and G. N. Popa, "*Reduced Cost Low Speed Wind or Hydro Energy Conversion System with Twin Stator Windings Induction Generator*", 16th International Power Electronics and Motion Control Conference and Exposition, pp. 404-411, Antalya, Turkey 21-24, Sept. 2014.
11. L. N. Tutelea, S. I. Deaconu, N. Budișan and I. Boldea, "*Double Stator Winding Induction Generator for Wind and Hydro Applications: 2D-FEM Analysis and Optimal Design*", Power Electronics and Applications (EPE), 2013 15th European Conference on, pp 2732-2737.
12. L. N. Tutelea, I. Boldea, S. I. Diaconu, "*Parameter Optimal Identification of Dual Three Phase Stator Winding Induction Machine*", OPTIM 2014, Brasov, Romania, pp. 231-238.